Finite Difference Elastic Modeling in 2.5D

F. Silva Neto[†], J. Costa[†], A. Novais[*] and B. Barbosa[†]

[*] Dept. of Applied Math., IMECC-UNICAMP, CP 6065, 13081-970 Campinas (SP), Brazil

[**] Geophysical Institute, UNICAMP, 13081-970 Campinas (SP), Brazil

[†] Geophysical Dept., Federal University of Pará, 66.075-110, Belém (PA), Brazil

This paper was prepared for presentation at the 9th International Congress of The Brazilian Geophysical Society held in Salvador, Brazil, 11-14 September 2005.

Abstract

Finite difference modeling of elastic wavefields in 2.5D is described in the velocity-stress formulation for isotropic media. The 2.5D modeling computes the 3-D elastic wavefield in a medium which is translation invariant in one coordinate direction. The approach is appealing due reduced storage and computing time when compared to full 3-D finite difference elastic modeling. The scheme handle inhomogeneities in mass density and elastic moduli, includes free-surface and perfect matched layers as absorbing boundaries. High order finite difference operator allows the use of a coarse mesh, reducing the storage even more without producing numerical dispersion and numerical anisotropy. Numerical experiments show the accuracy of the scheme and its computational efficiency. The method can also be extended to include anisotropy.

Introduction

The 3D elastic modeling of seismic wavefields is very expensive and requires extensive computational resources, even for a modest-sized model. If the modeling of 3D wave propagation is carried out in media with only 2D variations in the material properties, the seismic line being positioned within the symmetry plane, this is generally referred to as the 2.5D situation. This situation is very interesting to numerical experiments as the medium symmetry can be be used to reduce the complexity of the numerical task.

The modeling of seismic wave propagation in the 2.5D situation is helpful to approximately simulate situations where sources and receivers are located within the same plane. Some of the more common applications are conventional 2D seismic surveys, i.e., where the sources and receivers follow a single seismic line (Liner, 1991), and seismic borehole tomography (Pratt and Williamson, 1995).

Based on a Fourier transform of the acoustic wave equation in the out-of-plane direction, Song and Williamson(1995) presented an approach by repeated 2D finite-difference modeling in the frequency domain to find the exact solution of the 3D wave equation in the 2.5D situation for acoustic media with constant density, and applied their results to tomographic problems. They proved the quality of their results by a comparison to modeling with the Born approximation. Cao e Greenhalgh (1998) determined the stability and absorbing boundary conditions for this 2.5D FD approach, again for constant density, and compared the implementations in the time and frequency domains. In these papers, the inverse Fourier transform is carried out by a sum up to the Nyquist wavenumber. Recently, Novais and Santos (2004) revisited this approach and obtained stability conditions and sampling limits in the time domain as a function of the maximum wavenumber. In this work, we extend the time domain version of Novais and Santos (2005) to inhomogeneous elastic media. Moreover, we generalize the method to the computation of the complete elastic wavefield, composed of the three components of the particle velocity and the stress tensor field. We present the stability conditions for the corresponding higher-order finite-difference schemes and derive the perfect matched layer (PML) absorbing boundary conditions. Finally, we validate the 2.5D algorithm against 3D finite-difference modeling for an elastic extension of the Marmousi model.

Method

We use velocity and stress for representation of elastic wavefields. The velocity field, $v_i(\mathbf{x},t)$ and stress field, $\sigma_{ij}(\mathbf{x},t)$, must obey (Mittet, 2002)

$$\begin{aligned}\frac{\partial v_i(\mathbf{x},t)}{\partial t} &= \frac{1}{\rho(\mathbf{x})}\left[\frac{\partial \sigma_{i1}}{\partial x_1}+\frac{\partial \sigma_{i2}}{\partial x_2}+\frac{\partial \sigma_{i3}}{\partial x_3}\right] \\ &\quad +\frac{1}{\rho(\mathbf{x})} f_i(t)\delta(\mathbf{x}-\mathbf{x}_0) \qquad (1)\\ \frac{\partial \sigma_{ij}(\mathbf{x},t)}{\partial t} &= \lambda(\mathbf{x})\left(\frac{\partial v_1}{\partial x_1}+\frac{\partial v_2}{\partial x_2}+\frac{\partial v_3}{\partial x_3}\right)\delta_{ij} \\ &\quad +\mu(\mathbf{x})\left(\frac{\partial v_i}{\partial x_j}+\frac{\partial v_j}{\partial x_i}\right) \\ &\quad +q(t)\delta(\mathbf{x}-\mathbf{x}_0), \qquad (2)\end{aligned}$$

where $\rho(\mathbf{x})$ is density, $\lambda(\mathbf{x})$ and $\mu(\mathbf{x})$ are the Lamé parameters, f_i is the source force density, and q is the volume injection density rate. Assuming the material properties are translation invariant along the x_2 coordinate, we can express the wavefields as

$$v_i(x_1,x_2,x_3,t) = \int_{-\infty}^{+\infty} v_i(x_1,k_2,x_3,t)\,\exp(ik_2x_2)dk_2 \qquad (3)$$

$$\sigma_{ij}(x_1,x_2,x_3,t) = \int_{-\infty}^{+\infty} \sigma_{ij}(x_1,k_2,x_3,t)\,\exp(ik_2x_2)dk_2 \qquad (4)$$

Avoiding introducing new notational symbols, from now on $v_i \equiv v_i(x_1, k_2, x_3, t)$ and $\sigma_{ij} \equiv \sigma_{ij}(x_1, k_2, x_3, t)$. Substituting the expressions (3) and (4) into (1) and restricting the force density to the plane $x_2 = 0$ we obtain

$$\begin{aligned}
\frac{\partial v_1}{\partial t} &= \frac{1}{\rho}\left[\frac{\partial \sigma_{11}}{\partial x_1} + i\kappa_2\sigma_{12} + \frac{\partial \sigma_{13}}{\partial x_3}\right] + \frac{1}{\rho}f_1(t)\delta(\mathbf{X}-\mathbf{X}_0)\\
\frac{\partial v_2}{\partial t} &= \frac{1}{\rho}\left[\frac{\partial \sigma_{12}}{\partial x_1} + i\kappa_2\sigma_{22} + \frac{\partial \sigma_{23}}{\partial x_3}\right]\\
\frac{\partial v_1}{\partial t} &= \frac{1}{\rho}\left[\frac{\partial \sigma_{13}}{\partial x_1} + i\kappa_2\sigma_{23} + \frac{\partial \sigma_{33}}{\partial x_3}\right] + \frac{1}{\rho}f_3(t)\delta(\mathbf{X}-\mathbf{X}_0)
\end{aligned}$$

where $\mathbf{X} \equiv (x_1, x_3)$, $\rho \equiv \rho(\mathbf{X})$ and $\mathbf{X}_0$ is the source position in the plane $x_2 = 0$. Similarly, for the stress tensor

$$\begin{aligned}
\frac{\partial \sigma_{11}}{\partial t} &= \lambda\left(\frac{\partial v_1}{\partial x_1} + i\kappa_2 v_2 + \frac{\partial v_3}{\partial x_3}\right)\\
&\quad +2\mu\frac{\partial v_1}{\partial x_1} + q(t)\delta(\mathbf{X}-\mathbf{X}_0)\\
\frac{\partial \sigma_{22}}{\partial t} &= \lambda\left(\frac{\partial v_1}{\partial x_1} + i\kappa_2 v_2 + \frac{\partial v_3}{\partial x_3}\right)\\
&\quad +2\mu i\kappa_2 v_2 + q(t)\delta(\mathbf{X}-\mathbf{X}_0)\\
\frac{\partial \sigma_{33}}{\partial t} &= \lambda\left(\frac{\partial v_1}{\partial x_1} + i\kappa_2 v_2 + \frac{\partial v_3}{\partial x_3}\right)\\
&\quad +2\mu\frac{\partial v_3}{\partial x_3} + q(t)\delta(\mathbf{X}-\mathbf{X}_0)\\
\frac{\partial \sigma_{23}}{\partial t} &= \mu\left(\frac{\partial v_2}{\partial x_3} + i\kappa_2 v_3\right)\\
\frac{\partial \sigma_{13}}{\partial t} &= \mu\left(\frac{\partial v_1}{\partial x_3} + \frac{\partial v_3}{\partial x_1}\right)\\
\frac{\partial \sigma_{12}}{\partial t} &= \mu\left(\frac{\partial v_2}{\partial x_1} + i\kappa_2 v_1\right)
\end{aligned}$$

where $\lambda \equiv \lambda(\mathbf{X})$ and $\mu \equiv \mu(\mathbf{X})$.

The symmetry of the medium and the sources around the plane $x_2 = 0$ has the following consequency on the velocity field $v_2(x_1, -x_2, x_3) = -v_2(x_1, x_2, x_3)$, therefore $v_2(x_1, k_2, x_3)$ is a pure imaginary quantity. Defining the real quantities,

$$\begin{aligned}
u_2(x_1, \kappa_2, x_3) &\equiv iv_2(x_1, \kappa_2, x_3),\\
\tau_{12}(x_1, \kappa_2, x_3) &\equiv i\sigma_{12}(x_1, \kappa_2, x_3),\\
\tau_{23}(x_1, \kappa_2, x_3) &\equiv i\sigma_{23}(x_1, \kappa_2, x_3),
\end{aligned}$$

the final equations for 2.5D elastic modeling are

$$\begin{aligned}
\frac{\partial v_1}{\partial t} &= \frac{1}{\rho}\left[\frac{\partial \sigma_{11}}{\partial x_1} + \kappa_2\tau_{12} + \frac{\partial \sigma_{13}}{\partial x_3}\right] + \frac{1}{\rho}f_1(t)\delta(\mathbf{X}-\mathbf{X}_0)\\
\frac{\partial u_2}{\partial t} &= \frac{1}{\rho}\left[\frac{\partial \tau_{12}}{\partial x_1} - \kappa_2\sigma_{22} + \frac{\partial \tau_{23}}{\partial x_3}\right]\\
\frac{\partial v_1}{\partial t} &= \frac{1}{\rho}\left[\frac{\partial \sigma_{13}}{\partial x_1} + \kappa_2\tau_{23} + \frac{\partial \sigma_{33}}{\partial x_3}\right] + \frac{1}{\rho}f_3(t)\delta(\mathbf{X}-\mathbf{X}_0)\\
\frac{\partial \sigma_{11}}{\partial t} &= \lambda\left(\frac{\partial v_1}{\partial x_1} + \kappa_2 u_2 + \frac{\partial v_3}{\partial x_3}\right)\\
&\quad +2\mu(\mathbf{x})\frac{\partial v_1}{\partial x_1} + q(t)\delta(\mathbf{X}-\mathbf{X}_0)\\
\frac{\partial \sigma_{22}}{\partial t} &= \lambda\left(\frac{\partial v_1}{\partial x_1} + \kappa_2 u_2 + \frac{\partial v_3}{\partial x_3}\right)\\
&\quad +2\mu\kappa_2 u_2 + q(t)\delta(\mathbf{X}-\mathbf{X}_0)\\
\frac{\partial \sigma_{33}}{\partial t} &= \lambda\left(\frac{\partial v_1}{\partial x_1} + \kappa_2 u_2 + \frac{\partial v_3}{\partial x_3}\right)\\
&\quad +2\mu\frac{\partial v_3}{\partial x_3} + q(t)\delta(\mathbf{X}-\mathbf{X}_0)\\
\frac{\partial \tau_{23}}{\partial t} &= \mu\left(\frac{\partial u_2}{\partial x_3} - \kappa_2 v_3\right)\\
\frac{\partial \sigma_{13}}{\partial t} &= \mu\left(\frac{\partial v_1}{\partial x_3} + \frac{\partial v_3}{\partial x_1}\right)\\
\frac{\partial \tau_{12}}{\partial t} &= \mu\left(\frac{\partial u_2}{\partial x_1} - \kappa_2 v_1\right)
\end{aligned}$$

These equations are solved by finite differences in a staggered grid (Levander, 1988) for each value of k_2. We used a second order approximation for the time derivatives and high order approximations for space derivatives. The velocity field components v_1 and v_3, for receivers located in the plane $x_2 = 0$, are computed using (3), which in this case reduces to

$$v_i(x_1, 0, x_3, t) = \int_{-\infty}^{+\infty} v_i(x_1, k_2, x_3, t)dk_2. \qquad (5)$$

The extension of this approach to anisotropic media where the plane $x_2 = 0$ is a plane of mirror symmetry is straightforward. In our implementation free-surface boundary condition is implemented at the top surface (Mittet, 2002) and PML absorbing boundaries (Chew and Liu, 1996) are imposed at the bottom and lateral boundaries. The PML equations are presented in the Apendix. The stability condition for the 3-D finite difference scheme (Costa et al., 2005) is

$$\Delta t \leq \sqrt{\frac{2}{3d_0^{(2)}}}\frac{\Delta x}{c_P} \qquad (6)$$

where is Δt the time step , Δx is the grid space, c_P is the P wave velocity and

$$d_0^{(2)} = \sum_{j=-N+1}^{N+1} d_j,$$

where d_j are the coefficientes of the finite difference operator for first derivatives, with N equal to the order of the finite difference approximation. If we require that the 2.5D scheme obeys (7) (Novais and Santos, 2005), we can determine the maximum value for the wavenumber (Silva Neto, 2004)

$$k_{2\max} \leq \frac{\sqrt{2d_0^{(2)}}}{\Delta x}. \qquad (7)$$

The wavenumber sampling is $\Delta k_2 = 2\pi/\min(N_1, N_3)$ where N_1 is the number of grid points in x_1 direction and likewise for N_3. Using FD schemes of order higher than 12 the spatial sampling to avoid numerical dispersion must be

$$\Delta x \leq \frac{1}{3}\frac{C_{S\min}}{f_{\max}},$$

where $C_{S\min}$ is the minimum S wave velocity and $f_{\max}$ is the limit of the wavelet frequency band.

Numerical Experiments

We computed the elastic wavefield in a homogeneous halfspace with a free-surface produce by a point volume injection source. The model has density 2000 kg/m3, P wave

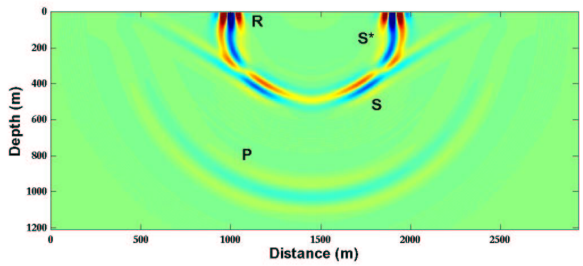

Figure 1: Vertical component of velocity wavefield after 0.5 s of propagation in a homogeneous half space with a free-suface, computed by 2.5D elastic modeling. The Rayleigh wave (R), P wave, S wave and the S* wave are labeled.

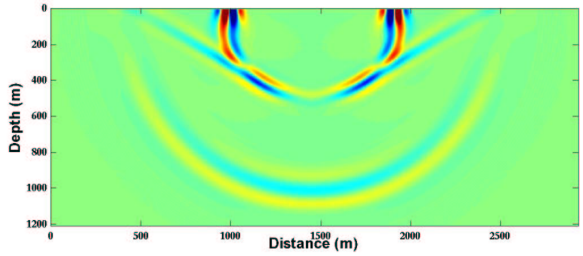

Figure 2: Vertical component of the velocity wavefield after 0.5 s of propagation computed using 2D elastic modeling. Observe the differences in the pulse width and shape and the relative amplitues among the events as compared with the 2.5D result.

velocity 2500 m/s and S wave velocity 1200 /s. The source is 10 m below the surface and the wavelet is a Ricker with 10 Hz of peak frequency. Figures 1 and 2 compare the results of 2.5D and 2D elastic modeling after 0.5 s of propagation. These figures show the differences in relative amplitudes and wave shape among events. Figure 3 shows the snapshot of the velocity field after 0.6 s computed using the 2.5D algorithm. We observe the good performance of PML absorbing boundary.

We used the the portion of the Marmousi model in Figure 3 to validate our method in a inhomogeneous model. We compared the results of the 2.5D FD scheme proposed and a full 3D velocity-stress FD modeling. The model density was computed from the P wave velocity using the Gardner formula (Gardner et al. , 1977) . The S wave velocity was computed from the P velocity over square root of three. We resampled the original model in a 24 m spacing grid. The final 2D mesh used for the 2.D FD modeling has 121×201 grid points. The 3D model has 35 repeated sections of this 2D mesh along x_2 direction.

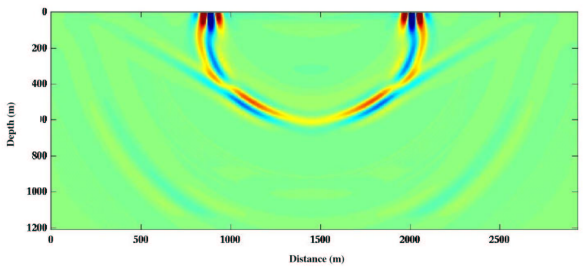

Figure 3: Vertical component of velocity wavefield after 0.6 s of propagation in a homogeneous half space with a free-suface, computed by 2.5D elastic modeling. The PML absorbing boundary condition performs well attenuating the P-wave at the bottom.

The volume injection source is located at the coordinates (3840 m , 20 m) and the wavelet was a Blackman-Harris with 6Hz of peak frequency. The receivers are located at every grid point from 480 m to 3360 m to grid points below the free-surface. The PML layers on the lateral boundaries and at the bottom of the model have width of 15 grid points.

The source specification is not the same for 2.5D and 3D FD. In the 3D FD the source spatially band limited, it is activated in small region around the source position to avoid numerical dispersion spatially modulated by a Blackman-Harris window. In the 2.5D scheme due to the Fourier transform the source is not spatially band limited in the x_2 direction but its spatially band limited in the 3D grid.

Figure 4 and Figure 5 present the horizontal and vertical component of the velocity field, respectively, at the receivers for the 2.5D and 3D modeling after 3s of propagation. The striking resemblance of the two sections can only be achieved if: (a) the two modeling schemes are equivalent; (b) the differences in the source modeling have minor impact on computed wavefields, and (c) if PML layers are very effective attenuating the wavefield at the boundaries.

Conclusions

Full 3D elastic FD modeling is challenging even for today's PC clusters. Our approach to 2.5D modeling computes the complete elastic wavefield and can be easily extended to accommodate anisotropy. Stability conditions and PML absorbing boundary conditions for the FD algorithm were derived. The algorithm was successfully validated in a complex inhomogeneous model against a full 3D elastic FD modeling. We believe this algorithm for 2.5D modeling is an accurate, low storage, alternative for seismic modeling whenever translation invariance along a strike direction can be assumed from geology. In such cases the 2.5D approach can compute the 3.D wavefield for models specified in dense grids in a single PC.

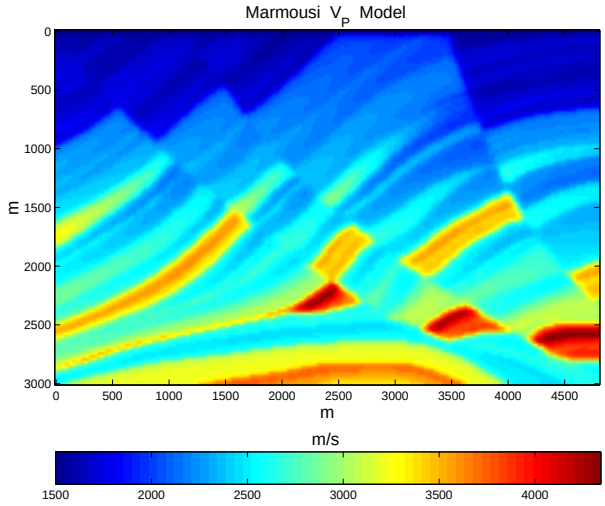

Figure 4: Marmousi P wave velocity model. For elastic modeling the density was computed using the Gardner formula and the S wave velocity is the P wave velocity over square root of three.

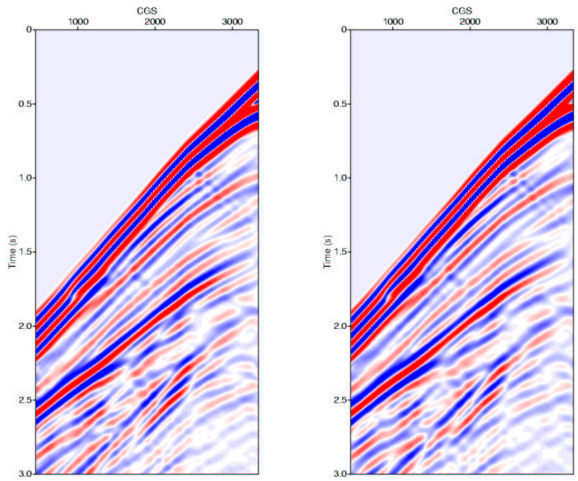

(a) (b)

Figure 5: Horizontal component of the velocity field after finite difference modeling; (a) using a 2.5D FD, and (b) using the 3D FD. The 2.5D result present higher frequency content because the source is not spatially band limited.

Acknowledgements

This work is supported by FINEP/CNPq and PETROBRAS through the project Rede Cooperativa de Pesquisa em Risco Exploratório. Brenda Barbosa has a scholarship from PRH-06/ANP.

References

Cao, S. e Greenhalgh, S., 1998. 2.5-d modeling of seismic wave propagation: Boundary condition, stability criterion, and e efficiency. Geophysics, Vol. 63, No. 6, p2082-2090.

Chew, W. C. e Liu, H. Q. ,1996. Perfectly matched layers for elastodynamics: A new absorbing boundary condition. J. Computational Acoust., Vol. 4 ,No 4, p72-79.

Costa, J., Novais, A., Silva Neto, F. A. and Tygel, M., 2005, 2.5D acoustic finite-difference modeling in variable density media, EAGE 67th Conference & Exhibition — Madrid, Spain.

Gardner, G. H. F., Gardner, L. F., and Gregory, A. F. ,1974. Formation velocity and density-the diagnostic basis for stratigraphic traps. Geophysics, Vol. 39, No 6, p770-780.

Levander, A. R.,1988, Fourth-order finite-difference P-SV seismograms. Geophysics, 53, No. 11, p. 1425-1436. Liner, C. L.,1991,Theory of a 2.5-D acoustic wave equation for constant density media. Geophysics , 56, No. 12, p.2114-2117.

Mittet, R., 2002, Free-surface boundary conditions for staggered-grid modeling schemes. Geophysics, 67, No 5, 1616-1623.

Novais, A. and Santos, L. T., 2005. 2.5-D finite-difference solution of the acoustic wave equation. Geophysical Prospecting .53, 1-9

Silva Neto, F. A. , 2004, Modelagem acústica por diferenças finitas e elementos finitos em 2-D e 2,5-D. Master Thesis , CPGF-UFPA.

Song, Z. e Williamson, P. R. ,1995. Frequency-domain acoustic-wave modeling and inversion of crosshole data: Part I - 2,5-D modeling method. Geophysics, Vol. 60 , No 3, p784-795.

Williamson, P. R. and Pratt, R. G. ,1995. A critical review of acoustic wave modeling procedures in 2.5-D dimension. Geophysics, Vol. 60 , No 2 , p591-595.

APPENDIX: Perfect Matched Layers (PML)

We use PML layers around the lateral and bottom boundaries of the model to reduce edge effects. Following Chew and Liu (1996), we assume the velocity wavefield at the PML layers is decomposed as

$$\begin{aligned} v_1 &= v_1^1 + v_1^2 + v_1^3, \\ u_2 &= u_2^1 + u_2^2 + u_2^3, \\ v_3 &= v_3^1 + v_3^2 + v_3^3, \end{aligned}$$

and accordingly the stress field

$$\begin{aligned} \sigma_{11} &= \sigma_{11}^1 + \sigma_{11}^2 + \sigma_{11}^3 \\ \sigma_{22} &= \sigma_{22}^1 + \sigma_{22}^2 + \sigma_{22}^3 \\ \sigma_{33} &= \sigma_{33}^1 + \sigma_{33}^2 + \sigma_{33}^3 \end{aligned}$$

$$\begin{aligned} \tau_{23} &= \tau_{23}^2 + \tau_{23}^3 \\ \sigma_{13} &= \sigma_{13}^1 + \sigma_{13}^3 \\ \tau_{12} &= \tau_{12}^1 + \tau_{12}^2 \end{aligned}$$

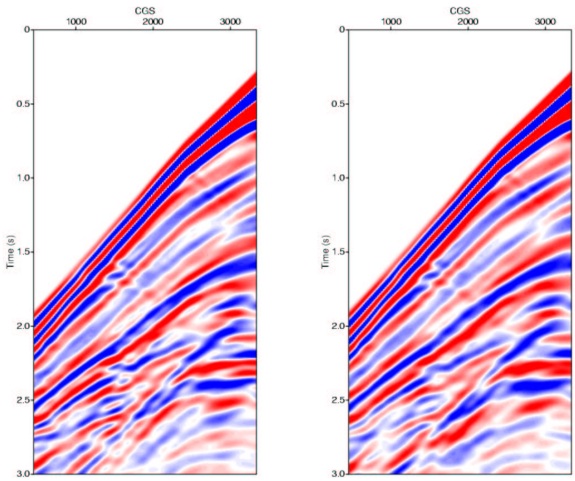

(a) (b)

Figure 6: Vertical component of the velocity field after finite difference modeling; (a) using a 2.5D FD, and (b) using the 3D FD. The 2.5D result present higher frequency content because the source is not spatially band limited.

where the superscripts indicate a coordinate direction. Using the complex stretch method of Chew and Liu (1996), we derived the following equations for the field components

$$
\begin{aligned}
\frac{\partial v_1^1}{\partial t} + \gamma_1(x_1) v_1^1 &= \frac{1}{\rho(\mathbf{X})}\left(\frac{\partial \sigma_{11}}{\partial x_1}\right) \\
\frac{\partial v_1^2}{\partial t} &= \frac{1}{\rho(\mathbf{X})}\kappa_2 \tau_{12} \\
\frac{\partial v_1^3}{\partial t} + \gamma_3(x_3) v_1^3 &= \frac{1}{\rho(\mathbf{X})}\left(\frac{\partial \sigma_{13}}{\partial x_3}\right) \\
\frac{\partial u_2^1}{\partial t} + \gamma_1(x_1) u_2^1 &= \frac{1}{\rho(\mathbf{X})}\left(\frac{\partial \tau_{12}}{\partial x_1}\right) \\
\frac{\partial u_2^2}{\partial t} &= -\frac{1}{\rho(\mathbf{X})}\kappa_2 \sigma_{22} \\
\frac{\partial u_2^3}{\partial t} + \gamma_3(x_3) u_2^3 &= \frac{1}{\rho(\mathbf{X})}\left(\frac{\partial \tau_{23}}{\partial x_3}\right) \\
\frac{\partial v_3^1}{\partial t} + \gamma_1(x_1) v_3^1 &= \frac{1}{\rho(\mathbf{X})}\left(\frac{\partial \sigma_{13}}{\partial x_1}\right) \\
\frac{\partial v_3^2}{\partial t} &= \frac{1}{\rho(\mathbf{X})}\kappa_2 \tau_{23} \\
\frac{\partial v_3^3}{\partial t} + \gamma_3(x_3) v_3^3 &= \frac{1}{\rho(\mathbf{X})}\left(\frac{\partial \sigma_{33}}{\partial x_3}\right) \\
\frac{\partial \sigma_{11}^1}{\partial t} + \gamma_1(x_1)\sigma_{11}^1 &= (\lambda(\mathbf{X}) + 2\mu(\mathbf{X}))\frac{\partial v_1}{\partial x_1} \\
\frac{\partial \sigma_{11}^2}{\partial t} &= \lambda(\mathbf{X})\kappa_2 u_2 \\
\frac{\partial \sigma_{11}^3}{\partial t} + \gamma_3(x_3)\sigma_{11}^3 &= \lambda(\mathbf{X})\frac{\partial v_3}{\partial x_3}
\end{aligned}
$$

$$
\begin{aligned}
\frac{\partial \sigma_{22}^1}{\partial t} + \gamma_1(x_1)\sigma_{22}^1 &= \lambda(\mathbf{X})\left(\frac{\partial v_1}{\partial x_1}\right) \\
\frac{\partial \sigma_{22}^2}{\partial t} &= (\lambda(\mathbf{X}) + 2\mu(\mathbf{X}))\,\kappa_2 u_2 \\
\frac{\partial \sigma_{22}^3}{\partial t} + \gamma_3(x_3)\sigma_{22}^3 &= \lambda(\mathbf{X})\left(\frac{\partial v_3}{\partial x_3}\right) \\
\frac{\partial \sigma_{33}^1}{\partial t} + \gamma_1(x_1)\sigma_{33}^1 &= \lambda(\mathbf{X})\left(\frac{\partial v_1}{\partial x_1}\right) \\
\frac{\partial \sigma_{33}^2}{\partial t} &= \lambda(\mathbf{X})\kappa_2 u_2 \\
\frac{\partial \sigma_{33}^3}{\partial t} + \gamma_3(x_3) &= (\lambda(\mathbf{X}) + 2\mu(\mathbf{X}))\left(\frac{\partial v_3}{\partial x_3}\right) \\
\frac{\partial \tau_{23}^2}{\partial t} &= -\mu(\mathbf{X})\kappa_2 v_3 \\
\frac{\partial \tau_{23}^3}{\partial t} + \gamma_3(x_3)\tau_{23}^3 &= \mu(\mathbf{X})\left(\frac{\partial u_2}{\partial x_3}\right) \\
\frac{\partial \sigma_{13}^1}{\partial t} + \gamma_1(x_1)\sigma_{13}^1 &= \mu(\mathbf{X})\left(\frac{\partial v_3}{\partial x_1}\right) \\
\frac{\partial \sigma_{13}^3}{\partial t} + \gamma_3(x_3)\sigma_{13}^3 &= \mu(\mathbf{X})\left(\frac{\partial v_1}{\partial x_3}\right) \\
\frac{\partial \tau_{12}^1}{\partial t} + \gamma_1(x_1)\tau_{12}^1 &= \mu(\mathbf{X})\left(\frac{\partial u_2}{\partial x_1}\right) \\
\frac{\partial \tau_{12}^2}{\partial t} &= -\mu(\mathbf{X})\kappa_2 v_1
\end{aligned}
$$

the field attenuation at the absorbing boundaries are controlled by γ_1 and γ_3. For example, at the bottom γ_1 is zero and

$$
\gamma_3(x_3) = \begin{cases} \frac{(x_3 - x_3^0)^2}{L^2}, & if x_3 > x_3^0 \\ 0, & otherwise \end{cases}
$$

x_3^0 is the coordinate where the PML begins and L is its width. Likewise, for the lateral boundaries only γ_1 is not zero.